

Terraced spreading of nanometer-thin lubricant using molecular dynamics



Brooklyn A. Noble^a, Andrey Ovcharenko^b, Bart Raeymaekers^{a,*}

^a Department of Mechanical Engineering, University of Utah, Salt Lake City, UT 84112, USA

^b Western Digital Corporation, San Jose, CA 95138, USA

ARTICLE INFO

Article history:

Received 13 October 2015

Received in revised form

30 December 2015

Accepted 4 January 2016

Available online 6 January 2016

Keywords:

Terraced spreading

Molecular dynamics

Perfluoropolyether lubricant

ABSTRACT

Ultra-thin lubricant films are essential in the design of nanoscale systems and devices as surface effects become increasingly important on the nanoscale. We have used molecular dynamics simulations to quantify terraced spreading of perfluoropolyether lubricant on a flat substrate as a function of polymer chain length, lubricant thickness, and functional end groups of the lubricant and the substrate. In addition, we have investigated the physical mechanisms that drive terraced lubricant spreading on a flat substrate. The results show that terraced lubricant spreading follows a process of diffusion and instability, where functional lubricant end groups are attracted to other functional end groups to form clusters that organize into layers. These distinct layers of functional end groups cause the lubricant thickness profile to take on a terraced shape, where layers correspond to the locations at which terraced formations occur. The presence of functional end groups determines the locations of both layer and terrace formations, and greatly affects lubricant spreading.

© 2016 Elsevier Ltd. All rights reserved.

1. Introduction

Ultra-thin lubricant films are of primary concern in the design of nanoscale systems and devices, as surface effects including adhesion and friction forces become increasingly important on the nanoscale [1]. As such, ultra-thin lubricant films are used in a myriad of nanoscale engineering applications and devices, including micro and nanoelectromechanical systems (MEMS/NEMS) [2], nanoimprint lithography [3], anti-biofouling [4], and hard disk drives (HDD) [5], which are ubiquitous in consumer electronics, automobiles, and medical devices, amongst others. However, designing complex ultra-thin film lubrication approaches to successfully solve nanoscale lubrication problems requires a fundamental understanding of the physical behavior of these ultra-thin lubricant films and the interaction with their environment. Thus, different aspects of nanometer-thin lubricant films have been studied, including lubrication [6], wetting [7], film evaporation [8], heat management [9], corrosion prevention [10], and spreading [11]. This paper focuses on understanding the physical mechanisms of nanoscale polymer-based lubricant spreading.

Experimental and numerical studies of different aspects of ultra-thin film, polymer-based lubricant spreading on a substrate have been documented in the literature. Several experiments with perfluoropolyether (PFPE) lubricant have demonstrated the formation of an approximately 1.5 nm precursor film on the substrate [12], also referred to as a foot, and defined as a molecularly-thin layer that spreads outward, preceding the main droplet. Mate [13] observed PFPE lubricant droplet spreading on a smooth amorphous carbon substrate using ellipsometry, and found that the spreading kinetics slow down for lubricants that are terminated with functional hydroxyl end groups (Zdol, Ztetraol) compared to nonfunctional lubricants (Z). Ma et al. [14] also studied the spreading of functional and nonfunctional ultra-thin PFPE lubricant films on smooth amorphous carbon surfaces and documented a complex stepped, or terraced structure for the functional lubricant. The first terrace of 2.2 nm thick represents a precursor film or foot, similar to previous observations [12], and subsequent terraces were observed at 6.4 nm and 9.8 nm with respect to the substrate surface. No such formations were observed for spreading of nonfunctional lubricant [14]. Tyndall et al. [15] qualitatively described the origins of this terraced spreading by attributing measured variations in the disjoining pressure within the lubricant thickness profile to molecular layering induced by polar interactions between the functional end groups and the substrate.

* Corresponding author.

E-mail address: bart.raeymaekers@utah.edu (B. Raeymaekers).

As experiments become increasingly difficult with decreasing length scale, numerical simulations have been used to study the interaction between lubricant and substrate on the nanoscale. Coarse-grained bead spring (CGBS) molecular dynamics (MD) models, which average atomistic interactions for computational simplicity yet preserve the essence of the molecular structure, have been employed to study the properties of ultra-thin lubricant films. Researchers have modeled PFPE lubricant films to study their molecular structure, and have observed formation of bead layers due to substrate interactions [16,17]. Others have observed the effects of functional end groups, which tend to cluster due to the strong attraction of the hydroxyl end groups of functional PFPE molecules [18]. Chen et al. [19] and Guo et al. [20] used CGBS models of several different polymer-based lubricants, contained in a cell with periodic boundary conditions (the lubricant does not spread), to demonstrate that the functional hydroxyl end group density varies with distance from the substrate, indicating that the hydroxyl groups conglomerate into molecular layers. Jhon et al. [21] showed that the variations of functional end group density become increasingly prominent with decreasing molecule length. Ogata et al. [22] analyzed PFPE lubricant surface morphology and found that the roughness of the lubricant surfaces decreases significantly when the amount of lubricant in the system formed a complete layer (lubricant thickness equal to 2 nm or 6–7 nm). Using a similar approach, Yi et al. [23] found that functional PFPE lubricant is unable to provide full substrate coverage for small lubricant quantities or when lubricant–substrate interactions are dominated by lubricant–lubricant interactions, as a strong attraction among lubricant molecules hinders surface diffusion.

Few researchers have attempted to model the nanoscale dynamics of lubricant spreading, including foot formations and molecular layering. Deb Nath et al. [24] used a CGBS model to observe the spreading of PFPE molecules and found that nonfunctional Z lubricant shows a more dispersive behavior than that of functional Zdol lubricant. Noble et al. [25] used a CGBS model to simulate spreading of a PFPE lubricant droplet on a flat substrate, and observed the formation of a foot, shoulder, and a vertical step for spreading of lubricant with functional hydroxyl groups, whereas they observed a hemispherical cap shape for spreading of nonfunctional lubricant, in agreement with several experiments [12,14]. Li et al. [26,27] also observed a single terraced profile and described the structure of functional lubricant droplets as having arched molecules near the substrate and the process of terraced spreading as a downward molecule movement in the outer regions of the droplet, diffusion of the foot, and molecule filling. This is in agreement with the work of Bekink et al. [28] who employed an MD model of simple molecules to show that lubricant spreading proceeds via downward mass transfer in the outer regions of a droplet whereas the center of the droplet experiences little mass transfer.

However, although experimentally observed, and critical to understanding the physical behavior of lubricant on the nanoscale, no publications seem to exist that clarify the physical mechanisms underlying the complexities of terraced lubricant spreading of polymer-based lubricants, and how these mechanisms govern lubricant spreading. This paper attempts to fill this gap and uses a CGBS molecular dynamics model to quantify terraced spreading on a flat substrate as a function of polymer chain length, lubricant thickness, and functional end groups of the lubricant and the substrate, and explain the physical mechanisms underlying terraced lubricant spreading on a flat substrate.

2. Methods

We have performed MD simulations of nanoscale polymer-based lubricant spreading on a flat substrate using a CGBS model

and the LAMMPS code [29,30]. Fig. 1(a) shows a schematic of the model. The PFPE lubricant first equilibrates between two walls (28 nm apart) that exert a Lennard Jones (LJ) interaction on the lubricant for 6.3 ns and then, after removal of the walls, spreads on a flat substrate for 250 ns. The initial position of the lubricant between the two walls is determined as follows. We select the initial position of the first bead of every molecular chain using a quasi-random distribution [31] and the initial position of the additional beads belonging to each molecular chain using a random walk approach, starting from the initial bead. Two types of lubricant are considered, both of which have a backbone structure of $X - [(O-CF_2 - CF_2)_p - (O-CF_2)_q] - O - X$ where $(p/q \cong 2/3)$. Zdol lubricant is terminated with a functional end group, i.e., $X = CF_2-CH_2 - OH$, and Z lubricant is terminated with a nonfunctional end group, i.e., $X = CF_3$. Fig. 1(b) depicts the CGBS model for a Zdol molecule, consisting of backbone beads (red (in web version)) and terminated at each end with a functional end bead (green (in web version)), whereas Fig. 1(c) shows the Z molecule model, consisting of only backbone beads. Fig. 1 also depicts the flat substrate, which consists of three layers of beads in a rigid, cubic lattice structure composed of nonfunctional substrate beads (grey) and a fraction S_f of functional substrate beads (blue (in web version)) on the top layer only. The potential functions defined between the different beads are indicated in Fig. 1(b) and (c) using the corresponding equation numbers, and are similar to the validated potentials and parameters used in previous research [19–21,32,33]. A truncated, shifted LJ potential U_{LJ} exists between all lubricant beads, given by

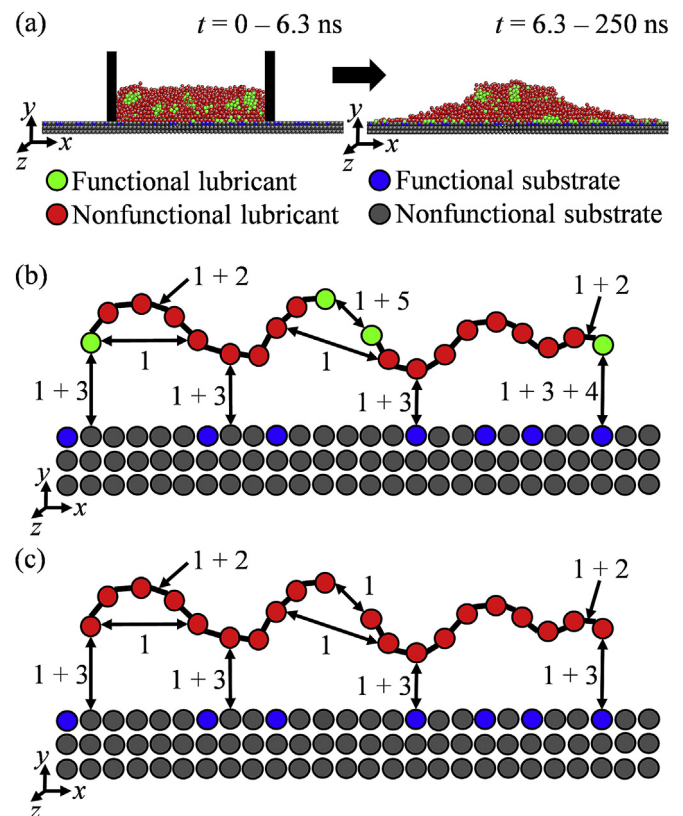


Fig. 1. (a) Schematic of the simulation showing the initial configuration at $t = 0$ and resulting configuration after lubricant spreading at $t = 250$ ns. (b) Schematic of coarse-grained bead spring model potential interactions for Zdol lubricant and (c) for Z lubricant. The numbers refer to the equations describing the bead interactions.

$$U_{LJ}(r) = 4\epsilon \left[\left(\frac{\sigma}{r} \right)^{12} - \left(\frac{\sigma}{r} \right)^6 - \left(\frac{\sigma}{r_c} \right)^{12} + \left(\frac{\sigma}{r_c} \right)^6 \right], \quad (1)$$

where r is the distance between two beads, $\sigma = 0.7$ nm is the bead diameter, $r_c = 2.5\sigma$ is the cutoff distance within which interactions between neighboring beads are considered, and $\epsilon = Tk_B$ is the potential well depth, where $T = 300$ K is the absolute temperature and k_B is the Boltzmann constant. A finitely extensible nonlinear elastic (FENE) potential U_{FENE} acts like a spring to bond neighboring beads of the same molecular chain, i.e.,

$$U_{FENE}(l) = -\frac{1}{2}kR_0^2 \ln \left[1 - \left(\frac{l-l_0}{R_0} \right)^2 \right], \quad (2)$$

where l is the bond length, $l_0 = 1.3\sigma$ is the equilibrium bond length, $R_0 = 0.3\sigma$ indicates the maximum extensible range, and $k = 40\epsilon/\sigma^2$ is the spring constant. The substrate interacts with the lubricant molecules, and attracts lubricant backbone beads via a dispersive van der Waals interaction $U_{bb-wall}$, described as

$$U_{bb-wall}(z) = 4\epsilon \left[\frac{1}{2} \left(\frac{\sigma}{z} \right)^9 - \frac{3}{2} \left(\frac{\sigma}{z} \right)^3 \right], \quad (3)$$

where z is the distance between a substrate bead and a lubricant bead. To model the attraction between functional polar end beads, we employ a short-range exponential potential U_{eb-eb} ,

$$U_{eb-eb}(r) = -2\epsilon \exp\left(-\frac{r-r_c}{d}\right), \quad (4)$$

where $r_c = 1.0\sigma$ is the cutoff distance and $d = 0.3\sigma$ is the decay length. Additionally, a fraction S_f of the substrate beads is functional, and an attractive force exists between functional substrate and functional lubricant beads, also modeled by a short-range exponential potential $U_{eb-wall}$,

$$U_{eb-wall}(z) = -2\epsilon \exp\left(-\frac{z-z_c}{d}\right), \quad (5)$$

where $z_c = 1.165\sigma$ is the cutoff distance. The substrate is rigid throughout the simulation and periodic boundary conditions exist in the z -direction (see Fig. 1). The lubricant is free to move according to the micro-canonical ensemble, and the temperature of the model is maintained at 300 K using a Langevin thermostat. A timestep of 0.03 ps is used throughout the simulation.

We have varied the lubricant molecule length $5 \leq N \leq 50$ beads for both lubricant types, while maintaining a constant bead mass of 0.2 kg/mole, thus effectively varying the molecular mass. The quantity of lubricant Q in the simulation, which determines the lubricant thickness, varies $5000 \leq Q \leq 40,000$ lubricant beads. The functional fraction of the substrate S_f , which defines the fraction of substrate beads that can bond to functional lubricant end beads, also varies $0\% \leq S_f \leq 100\%$. We quantify the formation of lubricant terraces on a flat substrate by measuring the lubricant thickness profile, obtained by low-pass filtering the maximum value of the lubricant y -coordinate (cutoff frequency of 0.2 [1/nm], based on spectral analysis) as a function of the x -coordinate (see coordinate system in Fig. 1). We quantify molecular layering in the spread lubricant by measuring the end bead density, defined as the number of end beads per unit volume, as a function of the y -coordinate. We also quantify molecular conformations in the lubricant by analyzing the anisotropic radius of gyration of the molecules as a function of the y -coordinate.

3. Results and discussion

Fig. 2(a) shows a typical result of a Zdol lubricant thickness profile after 250 ns of simulation, for $N = 5$, $Q = 20,000$, and $S_f = 100\%$. The black line represents the lubricant thickness profile and the black dots represent end beads. Fig. 2(b) shows the end bead density N_{eb}/σ^3 , defined as the number of end beads N_{eb} , per unit volume, after 250 ns of simulation, as a function of the nondimensional y -coordinate y/σ (black). The longitudinal (y -coordinate) radius of gyration R_{\perp} (blue (in web version)) is also shown as a function of the y -coordinate, and is defined as

$$R_{\perp}^2 = \frac{1}{N} \sum_{i=1}^N (y_i - y_g)^2, \quad (6)$$

where y_g is the y -coordinate of the molecule's center of mass and y_i is the y -coordinate of the i th bead belonging to that molecule. The lines represent a spline fit to the data points.

From Fig. 2(a), we clearly identify a foot and two terraces at $y/\sigma = 3$, 8.5, and 13.5, respectively, corresponding to $y = 2.1$ nm, 6.0 nm, and 9.5 nm, which is in good agreement with experimental observations of a step and terraces at approximately 2.0 nm, 5.5 nm, and 9.0 nm for Zdol lubricant (1860 g/mol) spreading on an amorphous carbon-coated aluminum substrate [14]. We also observe molecular layering, indicated by horizontal bands of conglomerated end beads, similar to previous results [19,21]. From Fig. 2(b), we observe that peaks in the end bead density occur as a result of molecular layering. Thus, the location of lubricant molecular layers is quantified as the local maxima of end bead density as a function of the y -coordinate. Additionally, when comparing the end bead density as a function of the y -coordinate to the spread lubricant thickness profile, we observe that the occurrence of end bead density peaks correlates with the locations where terraces form such that terraces manifest around end bead layers. Thus, the first minimum in the end bead density corresponds to the foot height, and subsequent minima correspond to the terrace heights in the spread lubricant profiles. This is accurate for distinct layers, such as between the foot and the second layer. However, slight deviation may exist as a result of imperfect layer formation, observed by the end beads located in the droplet exterior between the second and third layers.

We also observe that the longitudinal radius of gyration of the

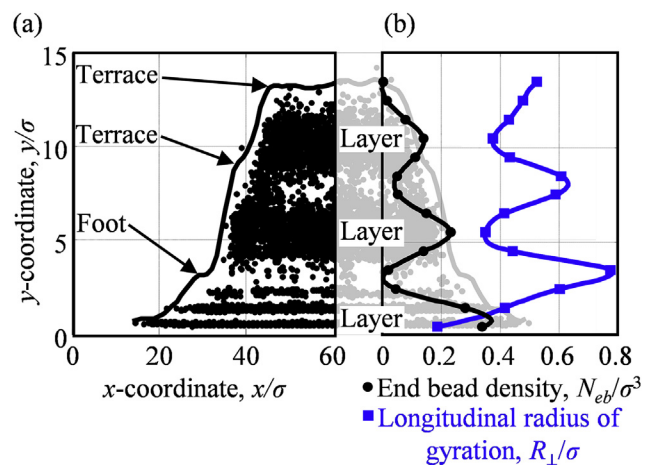


Fig. 2. (a) Typical example of lubricant thickness profile (Zdol, $N = 5$, $Q = 20,000$, $S_f = 100\%$) with end beads indicated as black dots, showing end bead layers, foot, and terrace formations. (b) Corresponding lubricant end bead density N_{eb}/σ^3 and longitudinal radius of gyration R_{\perp} as a function of the y -coordinate y/σ .

molecules is not uniform throughout the lubricant film as a result of molecular layering; minima of the end bead density correspond to maxima of the longitudinal component of the radius of gyration and vice versa. This indicates that molecule conformation is oblate where end bead maxima occur, whereas the molecules orient upright in between end bead density maxima. This explains that end beads form horizontal layers where oblate conformations are observed, and molecules span the gap between these layers in order to reach end bead clusters.

Fig. 3 shows the end bead density, after 250 ns of simulation, as a function of the nondimensional y -coordinate for molecule lengths $N = 5, 10, 20,$ and 50 beads, for both Zdol and Z lubricant, and for $S_f = 100\%$. The quantity of lubricant is varied $5000 \leq Q \leq 40,000$ for each molecule length. In Fig. 3, the black lines denote Z lubricant and colored lines denote Zdol lubricant. Only one case ($Q = 5000$ lubricant beads) is shown for Z lubricant because we find the spreading dynamics for Z lubricant to be independent of lubricant quantity and resulting film thickness, given sufficient spreading area. Insets show the thickness profile of the spread lubricant for each molecule length N and each lubricant quantity Q after 250 ns. In these insets, the contour shows the shape of the spread lubricant, and each black dot represents an end bead. The insets in Fig. 3 also indicate the lubricant height (y -coordinate) at which the highest terrace occurs.

From Fig. 3, we observe that end bead density peaks occur for all molecular lengths and lubricant quantities. For all Zdol lubricant cases, an initial end bead density peak occurs near the substrate, as a result of the short range exponential attractive potential between

functional substrate and lubricant end beads, in addition to the strong van der Waals attraction that exists between the substrate and all lubricant beads. The former causes end beads to bond to the substrate while the latter attracts all lubricant beads, creating the foot formation also observed in previous research [12,14]. Thus, we observe an increased density of functional end beads and non-functional backbone lubricant beads near the substrate. This locally increased density of lubricant beads, due to the presence of the substrate, locally increases the pressure in the lubricant film, which is in agreement with the disjoining pressure measurements by Tyndall et al. [15].

We also observe that for Zdol lubricant of constant molecule length (Fig. 3 (a), (b), (c), or (d)), end bead density peaks occur at approximately the same y -coordinate location for different lubricant quantities (different curves within Fig. 3(a–d)) and that the distance between peaks is nearly constant. However, the end bead density peaks do not occur at the same location for different lubricant molecule lengths. This is due to the attractive potential between functional Zdol end beads, which causes end beads to form clusters and backbone beads to form loops that orient away from the end bead clusters [25]. Occasionally, one molecule chain straddles two end bead clusters with one end bead belonging to each cluster. Hence, the length of the molecule determines the distance between end bead clusters, from which end bead layers form.

We observe that for $N = 5$ (Fig. 3(a)) the distance between end bead layers is approximately the molecular chain length. However, for $N > 5$ (Fig. 3(b–d)) the distance between layers does not

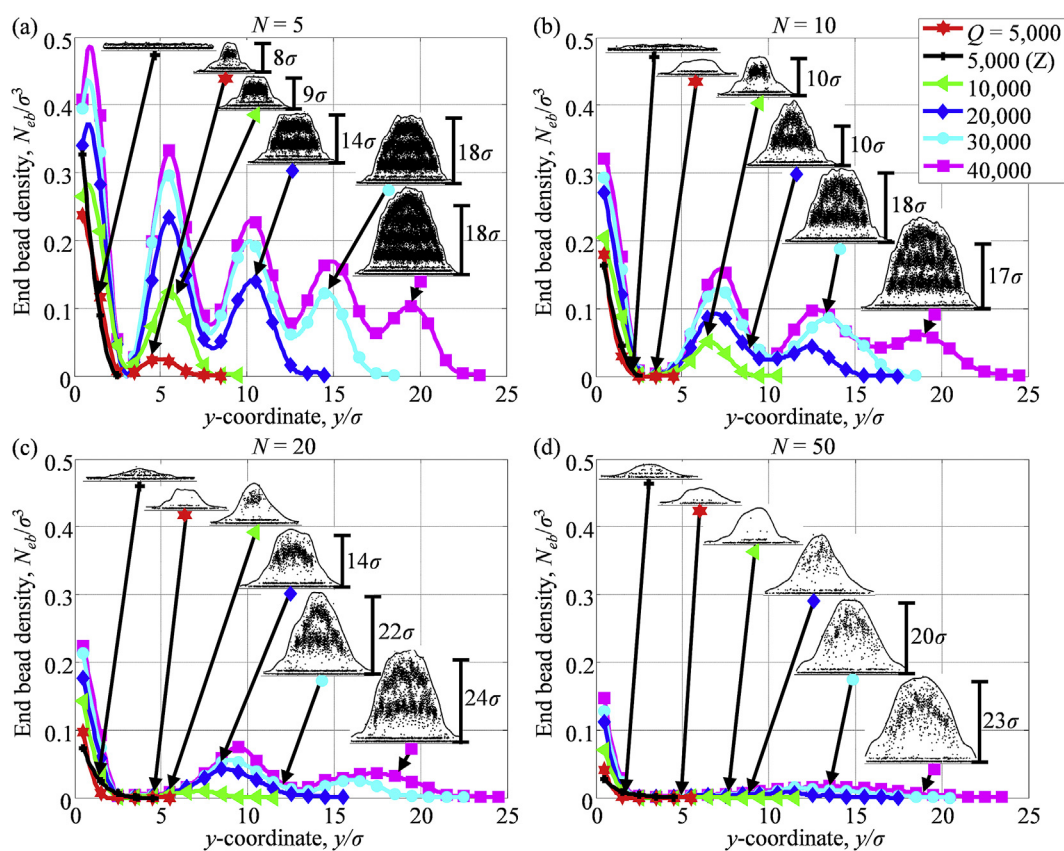


Fig. 3. Z (black) and Zdol (colored) lubricant end bead density N_{eb}/σ^3 as a function of the y -coordinate y/σ for lubricant quantities $5000 \leq Q \leq 40,000$ lubricant beads, percent functional substrate $S_f = 100\%$, and molecule lengths (a) $N = 5$, (b) $N = 10$, (c) $N = 20$, (d) $N = 50$ lubricant beads. Insets show the thickness profile, location of highest terrace, and location of end beads for each molecule length and quantity of lubricant after 250 ns of simulation. (For interpretation of the references to colour in this figure legend, the reader is referred to the web version of this article.)

increase proportionally with increasing molecular chain length due to entanglement of the lubricant backbone as well as the inability of a longer molecule to vertically support itself, which we have found to increase significantly for $N \geq 20$ [25]. We observe that the distance between end bead density peaks scales as the square root of molecule length (with a coefficient of determination $R^2 = 0.987$) for the molecule lengths tested. For Zdol cases where multiple end bead peaks occur ($Q \geq 20,000$ for Fig. 3(a) and (b), $Q \geq 30,000$ for Fig. 3(c)), the magnitude of the peaks decreases slightly with increasing y -coordinate for the same lubricant quantity and molecule length, because a layer of end beads can only support another layer that is smaller than itself. Thus, the end bead density of any particular layer decreases with increasing number of layers. Also, the magnitude of the end bead density peaks increases with increasing lubricant quantity for a constant molecule length, because more end beads are present in the model and the end bead layers grow proportionally. The magnitude of the end bead density peaks decreases with increasing molecule length for constant lubricant quantity, because only two end beads exist on each molecule and the number of lubricant beads, as opposed to number of molecular chains, is kept constant. Hence, the total number of end beads decreases with increasing molecule length. Similarly, the number of end bead density peaks decreases with increasing molecule length, for constant lubricant quantity. This is due, in part, to the decrease in total number of end beads with increasing molecule length. Also, it becomes more difficult for a molecular chain to straddle two end bead layers when the molecular length $N \geq 20$ beads, because of the entanglement of the backbone chain and the inability of a longer molecule to vertically support itself. This is in agreement with the results of Jhon et al. [21], which show that variations in end group density are more prominent for smaller molecules.

For nonfunctional Z lubricant, we observe no terrace formations. One end bead density peak occurs near the substrate, corresponding to a foot (pre-cursor film) formation. This is due to the short range van der Waals attraction that exists between the substrate and all lubricant beads, rather than the end bead attraction to the substrate, as in the case of Zdol. The Z end beads are distributed uniformly throughout the lubricant. An end bead peak occurs in this case because there is a higher density of total lubricant near the surface, which inherently corresponds to a higher density of end beads. In the case of Z lubricant, Fig. 3 insets show that molecular chains adhere tightly to the surface for small molecule lengths, $N < 20$, but appear like a hemispherical cap shape on the substrate, for large molecule lengths, $N \geq 20$, due to entanglement.

Fig. 4(a) – (f) shows an example (Zdol, $N = 5$, $Q = 20,000$, $S_f = 100\%$) that sequentially illustrates the physical mechanisms driving terraced lubricant spreading in Zdol lubricant. Fig. 4(a) represents the simulation just before spreading (time $t = 6.3$ ns) and Fig. 4(f) represents the simulation after spreading (time $t = 250$ ns). Lubricant slices, 3σ in width, document the spreading mechanism, where green circles represent functional end beads and red lines represent lubricant backbone beads. Blue and gray circles indicate functional and nonfunctional substrate beads, respectively, and grey rectangles (superimposed on the image for clarity) indicate the walls that initially contain the lubricant. Insets show velocity vectors of the beads in the area indicated.

From Fig. 4(a), we observe two vertical walls that exert an LJ interaction on the lubricant, containing the lubricant like a pipette. All lubricant molecules are attracted to the surface due to the dispersive van der Waals force, but functional end beads are attracted with an additional short range exponential potential, causing the end bead density near the substrate to be very high (green end beads are most densely packed near the substrate). End beads are attracted to each other due to the short range exponential

force that exists between functional end beads, which causes end beads to coagulate and form clusters that organize into layers, as indicated. Backbone bead chains form loops that orient away from the end bead clusters (arched, red backbone lines are most visible near the lubricant surface) and some lubricant chains span the gap between clusters, with one functional bead belonging to each cluster (red backbone lines span the gap between two adjacent layers). In Fig. 4(b) the vertical walls are removed. The lubricant molecules near the substrate that no longer experience the LJ attraction from the wall, are attracted to the surface, diffuse, and bond to the functional surface beads. This leads to the formation of a foot and increased lubricant density near the substrate. Simultaneously, end beads, which experience a strong attractive force to the substrate, repel backbone beads from the substrate. As a result of both of these mechanisms, the end bead density bonded to the substrate surface increases, as we have verified by analyzing the end bead density profile as a function of time. Other than the subtle motion of end beads pushing backbone beads away from the substrate, the lubricant near the substrate does not significantly change position and is not affected by removal of the vertical walls. Fig. 4(c), shows that the lubricant molecules that now belong to the foot left a void, causing the lubricant directly above the void to become unstable. Thus, an avalanche occurs and lubricant above the void diffuses down the sides of the droplet and either bonds to other end beads or bonds to the substrate, becoming part of the foot and filling the void. This is in qualitative agreement with the observations of Li et al. [26], which describe the process of terraced spreading as a downward molecule movement in the outer regions of the droplet, diffusion of the foot, and molecule filling. Similarly, in Fig. 4(d), the diffused lubricant that bonds to the surface or other end beads leaves a void, and another avalanche occurs as a result. From Fig. 4(e), we observe that the lubricant fills the void created by the avalanche by bonding to the surface or other end beads. This causes the end bead density of the lubricant bonded to the surface and other end bead clusters near the surface, i.e., the first layer, to increase. The small amount of lubricant remaining at the peak of the droplet is not stable, and soon absorbs into the nearest end bead cluster. Finally, Fig. 4(f) shows that lubricant motion slows and a steady state is approached. Distinct layers remain, causing the lubricant thickness profile to take on a stepped, or terraced formation. The inset of Fig. 4(f) shows almost no motion in the center of the droplet, which is in agreement with the work of Bekink et al. [28]. We refer to this area as an anchor, which is observed because spreading mainly proceeds via molecular diffusion in the outer regions of the droplet, as there is no force or instability in the center of the droplet that could drive lubricant away from the energy minimum achieved by bonding with the substrate.

Fig. 4 shows the case where four end bead layers reorganize into three as a result of spreading, but the process is the same for fewer layers, only step (d) does not occur, and for more layers, where steps (d) and (e) occur multiple times. This mechanism also agrees well with the experimental findings of Tyndall et al. [15], who describe foot and terrace formations in terms of disjoining pressure for the spreading of very thin films, using a finer resolution than that obtainable from a coarse-grained simulation approach. Near the surface, $y < 1.5$ nm, the disjoining pressure gradient is negative for both Z and Zdol due to the dispersive van der Waals disjoining pressure term, indicating that the lubricant wets the surface, referencing the diffusive foot formation [15]. In the case of Zdol, approximately 1.5 nm from the surface, the disjoining pressure gradient becomes positive due to the structural component of the disjoining pressure, indicating that spreading is absent and the lubricant de-wets, i.e., the formation of a terrace [15].

Fig. 5(a) shows the spread lubricant thickness profile and (b) the end bead density as a function of the y -coordinate for molecule

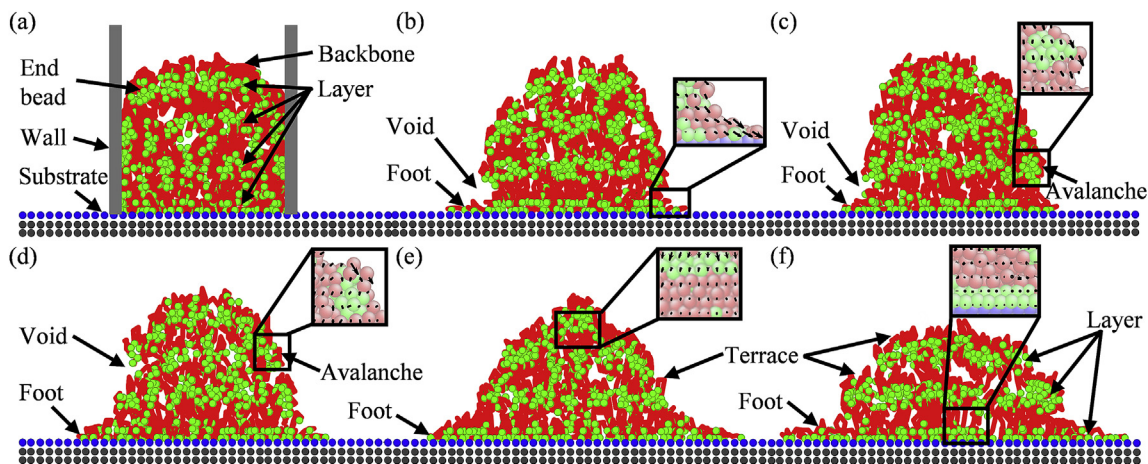


Fig. 4. Physical mechanisms that drive terraced lubricant spreading are demonstrated with a typical example (Zdol, $N = 5$, $Q = 20,000$, $S_f = 100\%$) of lubricant bead organization, where (a)–(f) occur sequentially. Thin slices of the lubricant droplet 3σ in width are shown where end beads are depicted as green circles and backbones beads are depicted as red lines. Insets show velocity vectors of beads in the area indicated. (For interpretation of the references to colour in this figure legend, the reader is referred to the web version of this article.)

length $N = 5$ and lubricant quantity $Q = 20,000$, for a functional fraction of the substrate $S_f = 0\%$, 50% , and 100% , after 250 ns of spreading of Zdol lubricant. We observe from Fig. 5(a) that an extremely diffusive foot exists for $S_f = 0\%$, and lubricant covers most of the substrate. However, for $S_f = 100\%$, the foot does not extend far beyond the base of the lubricant droplet. We also observe that the y -coordinate location of terrace formations are not significantly affected by the functional fraction of the substrate S_f . However, the quantity of lubricant in each layer is significantly less when the functional fraction of the substrate is small, due to the increased quantity of the lubricant belonging to the diffusive foot, and the

resulting larger spread diameter. From Fig. 5(b), we observe that in the case of a small functional fraction of the substrate, the locations of the end bead peaks are slightly shifted, again due to the larger foot formation. However, the locations of end bead density peaks are almost identical for the $S_f = 100\%$ and $S_f = 50\%$ cases.

The physical mechanisms that drive terraced spreading are similar for all cases where $S_f \neq 0\%$, but when $S_f = 0\%$, lubricant only interacts with the substrate via van der Waals forces; thus, lubricant end beads do not bond to the substrate. In our simulation, end bead clusters form and, when the vertical walls are removed at the beginning of the simulation, the lubricant molecules near the substrate that no longer experience the LJ attraction from the vertical wall, are attracted to the surface and diffuse. However, the lubricant molecules do not interact with the substrate as strongly as they would when $S_f \neq 0\%$ and, thus, an increasingly diffusive foot is observed with decreasing S_f . Similarly to the $S_f = 100\%$ case, an avalanche occurs that fills the void created by the diffused lubricant and the lubricant will either join another end bead cluster or become part of the diffusive foot. We observe an anchor, as there is no driving force acting on the lubricant in the center of the droplet. We also observe a larger spread lubricant diameter and, thus, the lubricant thickness decreases, which can only support smaller end bead layers compared to a thicker lubricant, as demonstrated in Fig. 3. This finding is contrary to our previous results [25] where spread lubricant diameter was only marginally affected by the fraction of functional substrate, S_f . In this previous study, significantly less lubricant was used and, therefore, the central droplet was not large enough to drive spreading. This finding is in agreement with the experimental results of Mate [13], which show that drastically different spreading kinetics occur when a central droplet is available to feed lubricant into a precursor film.

In the case of Z lubricant for any substrate functionality, a similar initial mechanism occurs when the walls are removed. Diffusion proceeds via downward molecular motion in the outer regions of the lubricant mass. However, in the case of Z lubricant, there is no end bead attraction to the substrate or other lubricant that would inhibit diffusion. Hence, spreading increases and the only mechanism that slows diffusion is molecular entanglement.

4. Conclusions

The quantity and location of high end bead density areas, i.e., molecular layer formations, correspond to the quantity and location

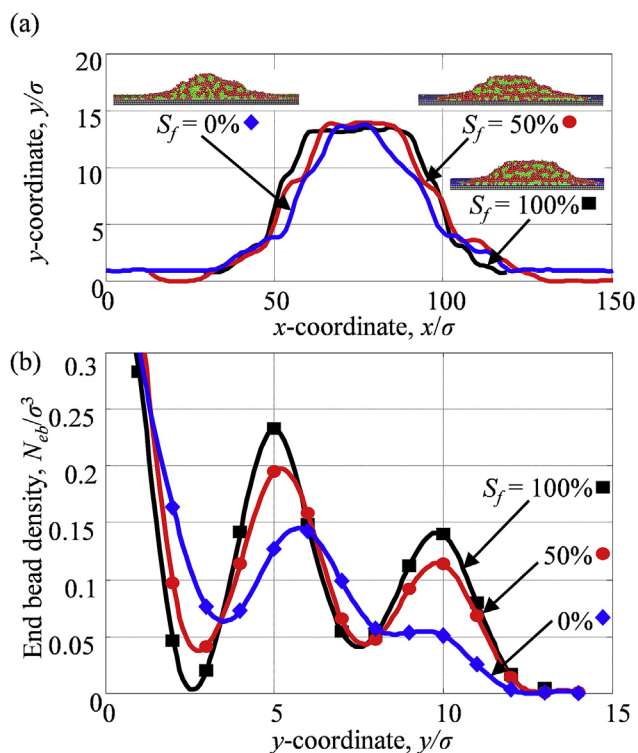


Fig. 5. (a) Lubricant thickness profile and (b) end bead density N_{eb}/σ^3 as a function of the y -coordinate y/σ for Zdol, $N = 5$, $Q = 20,000$, and $S_f = 0\%$, 50% , and 100% after 250 ns of simulation. Insets show a perspective view of the spread lubricant.

of terraced formations. The presence of functional end beads determines the presence of both layer formations and terrace formations, and greatly affects lubricant spreading. In the case of terraced lubricant spreading, molecule length and lubricant thickness, or quantity of lubricant, affect the number and location of layer formations, where small molecule lengths and large lubricant thicknesses result in the maximum number of terraces. The mechanism of terraced lubricant spreading for functional Zdol lubricant follows a process of diffusion and instability, where functional end beads are attracted to other functional end beads to form clusters that will organize into layers. The inception of spreading results in diffusion of the near-surface molecules on the outer edge of the droplet, which adhere to the substrate. This lubricant movement results in a void causing the lubricant above to become unstable and diffuse down the sides of the droplet, bonding to other clusters or to the surface and filling the void. This process of diffusion, followed by instability, is repeated until lubricant motion is slowed and a steady state is approached. Distinct layers remain, causing the lubricant thickness profile to take on a terraced profile.

Acknowledgments

This work was supported in part by Western Digital Corporation, San Jose, CA. Brooklyn Noble acknowledges support from a Department of Energy, National Nuclear Security Administration (NNSA), Stewardship Science Fellowship (SSGF), award DE-NA0002135. This work used the Extreme Science and Engineering Discovery Environment (XSEDE), which is supported by National Science Foundation grant number ACI-1053575. The support and resources from the Center for High Performance Computing at the University of Utah are gratefully acknowledged. Finally, the authors thank George W. Tyndall and C. Mathew Mate for helpful discussions.

References

- [1] I. Szlufarska, M. Chandross, R.W. Carpick, Recent Advances in single-asperity nanotribology, *J. Phys. D: Appl. Phys.* 41 (2008) 123001.
- [2] S.H. Kim, D.B. Asay, M.T. Dugger, Nanotribology and MEMS, *Nanotoday* 2 (5) (2007) 22–29.
- [3] J. Teisseire, A. Ravoux, M. Foresti, E. Barthel, Confinement and flow dynamics in thin polymer films for nanoimprint lithography, *Appl. Phys. Lett.* 98 (2011), 013106.
- [4] A.K. Epstein, T.-S. Wong, R.A. Belisle, E.M. Boggs, J. Aizenberg, Liquid-infused structured surfaces with exceptional anti-biofouling performance, *Proc. Natl. Acad. Sci. U.S.A.* 109 (33) (2012) 13182–13187.
- [5] B. Marchon, Lubricant design attributes for subnanometer head-disk clearance, *IEEE Trans. Magn.* 45 (2) (2009) 872–876.
- [6] W.W.F. Chong, M. Teodorescu, H. Rahnejat, Effect of lubricant molecular rheology on formation and shear of ultra-thin surface films, *J. Phys. D: Appl. Phys.* 44 (2011) 165302.
- [7] B. Saramago, Thin liquid wetting films, *Curr. Opin. Colloid Interface Sci.* 15 (2010) 330–340.
- [8] S. Narayanan, A.G. Fedorov, Y.K. Joshi, Interfacial transport of evaporating water confined in nanopores, *Langmuir* 27 (2011) 10666–10676.
- [9] O.A. Kabov, D.V. Zaitsev, V.V. Cheverda, A. Bar-Cohen, Evaporation and flow dynamics of thin, shear-driven liquid films in microgap channels, *Exp. Therm. Fluid Sci.* 35 (2011) 825–831.
- [10] A. Tomala, A. Karpinska, W.S.M. Werner, A. Olver, H. Stori, Tribological properties of additives for water-based lubricants, *Wear* 269 (2010) 804–810.
- [11] D. Bonn, J. Eggers, J. Indekeu, J. Meunier, E. Rolley, Wetting and spreading, *Rev. Mod. Phys.* 81 (2) (2009) 771–805.
- [12] Y. Mitsuya, H. Zhang, J. Ohgi, K. Fukuzawa, Experimental comparisons of spreading and replenishment flows of molecularly thin lubricant films coated on magnetic disks, *IEEE Trans. Magn.* 44 (11) (2008) 3641–3644.
- [13] C.M. Mate, Spreading kinetics of lubricant droplets on magnetic recording disks, *Tribol. Lett.* 51 (2013) 385–395.
- [14] X. Ma, J. Gui, L. Smoliar, K. Grannen, B. Marchon, Spreading of perfluoropolyether films on amorphous carbon surfaces, *J. Chem. Phys.* 110 (6) (1999) 3129–3137.
- [15] G.W. Tyndall, T.E. Karis, M.S. Jhon, Spreading profiles of molecularly thin perfluoropolyether films, *Tribol. Trans.* 42 (3) (1999) 463–470.
- [16] M. Fukuda, H. Zhang, T. Ishiguro, K. Fukuzawa, S. Itoh, Adhesion properties of nanometer-thick perfluoropolyether films confined between solid surfaces: a coarse-grained molecular dynamics study, *Tribol. Lett.* 51 (2013) 479–487.
- [17] J.-X. Yang, J. Koplik, J.R. Banavar, Terraced spreading of simple liquids on solid surfaces, *Phys. Rev. A* 46 (12) (1992) 7738–7749.
- [18] S. Ogata, Y. Mitsuya, H. Zhang, K. Fukuzawa, Molecular dynamics simulation for analysis of surface morphology of lubricant films with functional endgroups, *IEEE Trans. Magn.* 41 (10) (2005) 3013–3015.
- [19] H. Chen, Q. Guo, M.S. Jhon, Effects of molecular structure on the conformation and dynamics of perfluoropolyether nanofilms, *IEEE Trans. Magn.* 43 (6) (2007) 2247–2249.
- [20] Q. Guo, S. Izumisawa, D.M. Phillips, M.S. Jhon, Surface morphology and molecular conformation for ultrathin lubricant films with functional end groups, *J. Appl. Phys.* 93 (2003) 8707–8709.
- [21] M.S. Jhon, S. Izumisawa, Q. Guo, D.M. Phillips, Y.-T. Hsia, Simulation of nanostructured lubricant films, *IEEE Trans. Magn.* 39 (2) (2003) 754–758.
- [22] S. Ogata, H. Zhang, K. Fukuzawa, Y. Mitsuya, Quantification of the surface morphology of lubricant films with polar end groups using molecular dynamics simulations: periodic changes in morphology depending on film thickness, *J. Tribol.* 130 (2008), 022301.
- [23] T. Yi, U.S. Ramasamy, S. Lichter, A. Martini, Stability and structure of nanometer-thin perfluoropolyether films using molecular simulations, *Tribol. Lett.* 54 (2014) 119–127.
- [24] S.K. Deb Nath, C.H. Wong, V. Sorkin, Z.D. Sha, Y.W. Zhang, S.G. Kim, Study of the spreading of perfluoropolyether lubricants on a diamond-like carbon film, *Tribol. Trans.* 56 (2) (2013) 255–267.
- [25] B. Noble, A. Ovcharenko, B. Raeymaekers, Quantifying lubricant droplet spreading on a flat substrate using molecular dynamics, *Appl. Phys. Lett.* 105 (2014) 151601.
- [26] X. Li, Y. Hu, H. Wang, Functional perfluoropolyether spreading on a solid substrate, *J. Appl. Phys.* 100 (2006), 074901.
- [27] X. Li, Y. Hu, L. Jiang, Spreading dynamics of functional droplets, *Appl. Surf. Sci.* 255 (2008) 3336–3341.
- [28] S. Bekink, S. Karaborni, G. Verbist, K. Esselink, Simulating the spreading of a drop in the terraced wetting regime, *Phys. Rev. Lett.* 76 (1996) 3766–3769.
- [29] S. Plimpton, Fast parallel algorithms for short-range molecular dynamics, *J. Comput. Phys.* 117 (1995) 1–19.
- [30] J. Towns, T. Cockerill, M. Dahan, I. Foster, K. Gathier, A. Grimshaw, V. Hazlewood, S. Lathrop, D. Lifka, G.D. Peterson, R. Roskies, J.R. Scott, N. Wilkins-Diehr, XSEDE: accelerating scientific discovery, *Comput. Sci. Eng.* 16 (5) (2014) 62–74.
- [31] L. Kocis, W.J. Whiten, Computational investigations of low-discrepancy sequences, *ACM Trans. Math. Softw.* 23 (2) (1997) 266–294.
- [32] Q. Guo, S. Izumisawa, M.S. Jhon, Y.-T. Hsia, Transport properties of nanoscale lubricant films, *IEEE Trans. Magn.* 40 (4) (2004) 3177–3179.
- [33] Y.-T. Hsia, Q. Guo, S. Izumisawa, M.S. Jhon, The dynamic behavior of ultrathin lubricant films, *Microsyst. Technol.* 11 (2005) 881–886.